GPS Carrier Tracking Loop Performance in the presence of Ionospheric Scintillations

Todd E. Humphreys, Mark L. Psiaki, and Paul M. Kintner, Jr., *Cornell University, Ithaca, N.Y.*
Brent M. Ledvina, *Applied Research Laboratories, Austin, TX*

BIOGRAPHIES

Todd E. Humphreys is a graduate student in the Sibley School of Mechanical and Aerospace Engineering at Cornell University. He received his B.S. and M.S. in Electrical and Computer Engineering from Utah State University. His research interests are in estimation and filtering, spacecraft attitude determination, GPS technology, and GPS-based study of the ionosphere and neutral atmosphere.

Brent M. Ledvina is a Postdoctoral Associate at Applied Research Laboratories at the University of Texas at Austin. He received a B.S. in Electrical and Computer Engineering from the University of Wisconsin at Madison and a Ph.D. in Electrical and Computer Engineering from Cornell University. His research interests are in the areas of ionospheric physics, space weather, estimation and filtering, and GPS/GNSS technology and applications.

Mark L. Psiaki is an Associate Professor of Mechanical and Aerospace Engineering at Cornell University. He received a B.A. in Physics and M.A. and Ph.D. degrees in Mechanical and Aerospace Engineering from Princeton University. His research interests are in the areas of estimation and filtering, spacecraft attitude and orbit determination, and GPS technology and applications.

Paul M. Kintner, Jr. is a Professor of Electrical and Computer Engineering at Cornell University. He received a B.S in Physics from the University of Rochester and a Ph.D. in Physics from the University of Minnesota. His research interests include the electrical properties of upper atmospheres, space weather, and developing GPS instruments for space science. He is a Fellow of the APS.

ABSTRACT

The performance of several GPS carrier tracking loops is evaluated using wideband GPS data recorded during strong ionospheric scintillations. The aim of this study is to determine the loop structures and parameters that enable good phase tracking during the power fades and phase dynamics induced by scintillations. Constant-bandwidth and variable-bandwidth loops are studied using theoretical models, simulation, and tests with actual GPS signals. Constant-bandwidth loops with loop bandwidths near 15 Hz are shown to lose phase lock during scintillations. Use of the decision-directed discriminator reduces the carrier lock threshold by ∼1 dB relative to the arctangent and conventional Costas discriminators. A proposed variable-bandwidth loop based on a Kalman filter reduces the carrier lock threshold by more than 7 dB compared to a 15-Hz constant-bandwidth loop. The Kalman filter-based strategy employs a soft-decision discriminator, explicitly models the effects of receiver clock noise, and optimally adapts the loop bandwidth to the carrier-to-noise ratio. In extensive simulation and in tests using actual wideband GPS data, the Kalman filter PLL demonstrates improved cycle slip immunity relative to constant bandwidth PLLs.

INTRODUCTION

During the last decade, researchers have exploited Global Positioning System (GPS) signals to study the ionospheric dynamics connected with radio-frequency scintillations.[1–6] Proposals for future work call for large arrays of GPS receivers whose combined measurements will be used to determine the spatial irregularity, velocity, and height of the structures in the disturbed ionosphere. Such wide-area studies will require hundreds of GPS receivers specially designed to provide accurate carrier phase and amplitude data, and to hold tracking lock during the deep power fades and vigorous phase dynamics associated with scintillations. This paper focuses on a critical component that is commonly considered the weak link in these specially designed receivers: the carrier tracking loop.

Two GPS receivers specially designed for monitoring scintillations are reported in the open literature. The Cornell Scintillation Monitor employs a frequency-locked loop (FLL)[1,2] that is known to lose lock during strong equatorial scintillations.[7] The Ionospheric Scintillation Monitor (ISM) developed by GPS Silicon Valley employs a 3rd-order 10- or 15-Hz decision-directed arctangent phase-locked loop (PLL).[3,8,9] The ISM has been used successfully to monitor amplitude and phase scintillations at several locations,[4,5] but is known to lose lock during simulated (Ref. 10) and actual (Ref. 8) scintillations. The ISM's loop filter is optimal for the case of small phase error and additive white phase noise with a time-invariant noise intensity.[9,11] A strongly scintillating GPS carrier signal does not conform to these assumptions. For equatorial scintillations, the carrier-to-noise ratio (C/N_0) of a scintillating signal is strongly time-dependent. The result of this, as demonstrated herein, is that PLLs that employ wide-bandwidth loop filters (∼ 15 Hz) lose lock during strong equatorial scintillations.

Preprint of the 2005 ION GNSS Conference Long Beach, CA, September 13-16, 2005

The general theory of PLLs is a topic with much heritage.[11–16] The subject is treated from a GPS perspective in Refs. [17] and [18]. Much work has studied the characterization and optimization of the Costas-type loops used in GPS receivers (see Ref. [12], ch. 11, and Refs. [19–21]). Although none of these addresses tracking loops specifically designed for operation in a scintillating environment, their general results can be used to guide the design of a scintillation-robust PLL. In contrast to these previous studies, however, the present work does not assume that the carrier tracking loop's pre-detection bandwidth is much larger than its loop bandwidth. Relaxation of this assumption has important implications for loop stability and phase accuracy.

A characterization of GPS receiver performance during simulated scintillation is reported in Refs. [10] and [22], wherein modified Doppler and signal power time histories mimic the effects of scintillation on a GPS receiver connected to a GPS signal simulator. However, the test setup does not isolate the carrier tracking loops nor permit enough tests to clearly define the lock thresholds of the various receivers tested. Moreover, the scintillations in the raw wideband GPS digital data used to test the tracking loops in the current work are more realistic than the data-derived scintillations in Refs. [10] and [22].

This paper examines the threshold behavior of the constant-bandwidth PLL (CBPLL) and compares its performance with a variable-bandwidth PLL based on a Kalman filter (KFPLL). The comparative study is divided into three sections. In Section I, the relevant theory of the Costas PLL is reviewed and the KFPLL is introduced. This includes a discussion on loop structure and parameter optimization. In Section II, Monte-Carlo simulation is used to evaluate the performance of the PLLs. Results are compared to the theoretical predictions from step 1. In Section III, GPS signals recorded in Cachoeira Paulista, Brazil during strong ionospheric scintillations are used to evaluate the PLLs. The data set spans several hours and includes scintillations with S_4 index values of 0.9 that are associated with power fades of more than 30 dB. The data are processed using off-line implementations of the CBPLL (over a range of bandwidths) and the KFPLL. Remarks and conclusions follow in Sections IV and V.

This paper's contributions are (1) a unified analysis, based on theoretical models and on simulation, of Costas-type PLLs, specifically addressing parameters relevant to good loop operation during ionospheric scintillations, and (2) a performance evaluation of several tracking loops using actual GPS wideband digital data collected during strong scintillations.

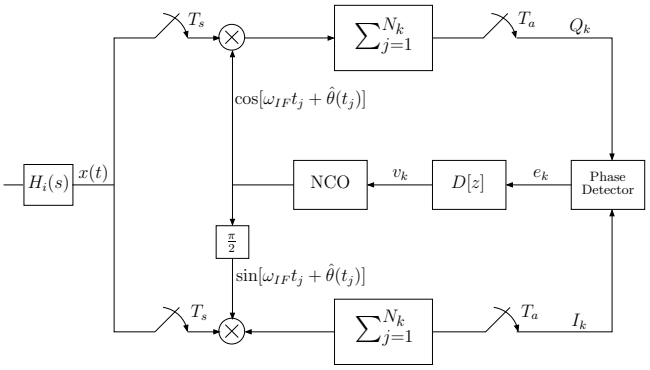

Fig. 1. Discrete-time Costas Loop functional diagram.

I. MODEL ANALYSIS

This section examines the tracking loop theory relevant to GPS receivers. Models are presented for a general class of CBPLLs and for the KFPLL. These models will provide intuition about the challenges involved in tracking scintillating signals.

A. The Costas Loop

The data bits on the transmitted GPS signal must be removed before the underlying carrier phase can be tracked. The Costas loop is employed for this purpose in GPS phase-tracking applications. A functional diagram for the discrete-time Costas loop is shown in Fig. 1.

The signal exiting the receiver's RF front-end is modeled as

$$x(t) = A(t)m(t)C(t)\sin[\omega_{IF}t + \theta(t)] + n_i(t) \qquad (1)$$

where $A(t)$ is the carrier amplitude, $m(t)$ is the 50-Hz binary data modulation, $C(t)$ is the 1.023-MHz binary C/A PRN bit stream, ω_{IF} is the RF front-end's intermediate image of the nominal GPS L1 carrier frequency, $\theta(t)$ is the carrier phase to be estimated, and $n_i(t)$ is a zero-mean additive Gaussian white noise process representing channel noise and quantization effects. The transfer function $H_i(s)$ models the effective band-pass filtering of the RF front-end. The process $n_i(t)$ is assumed to be spectrally flat with density $N_0/2$ within W_i, the two-sided bandwidth of $H_i(s)$.

For simplicity, this study will assume known symbol timing; that is, it is assumed that the delay-locked loop used to track the symbol transitions in $m(t)$ and $C(t)$ is operating in its tracking mode. Under this assumption, the receiver's replica of the C/A PRN code can be used to eliminate $C(t)$ from $x(t)$.

The signal $x(t)$ is sampled every $T_s \simeq 1/W_i$ seconds before correlation with the receiver's in-phase and quadrature carrier replicas. The sampled signal [with $C(t)$ omit-

ted] takes the form

$$x(t_j) = A(t_j)m(t_j)\sin[\omega_{IF}t_j + \theta(t_j)] + n_i(t_j) \quad (2)$$

where $n_i(t_j)$ is an element of a zero-mean discrete-time Gaussian white noise sequence with variance $\sigma^2_{n_i} = N_0/2T_s$. The carrier-to-noise ratio C/N_0 associated with $x(t_j)$ is

$$\frac{C}{N_0} = \frac{A^2}{4\sigma^2_{n_i}T_s} \quad (3)$$

The sampled signal $x(t_j)$ is reduced to baseband by correlation and accumulation in the in-phase and quadrature arms of the Costas loop. The accumulator output is sampled at $1/T_a$ Hz where $T_b \geq T_a >> T_s$, with T_b denoting the data bit period equal to 20 ms. The loop's predetection bandwidth is defined as $1/T_a$. Known symbol timing permits alignment of the accumulate-and-dump operation with data bit transitions. The accumulator outputs are modeled as

$$I_k = \frac{N_k\bar{A}_k m_l}{2}\cos(\bar{\varphi}_k) + n_{I,k} \quad (4a)$$

$$Q_k = \frac{N_k\bar{A}_k m_l}{2}\sin(\bar{\varphi}_k) + n_{Q,k} \quad (4b)$$

where $\bar{A}_k$ and $\bar{\varphi}_k$ are the average carrier amplitude and phase error over the accumulation interval, N_k is the number of samples in the kth accumulation interval, m_l is the current data bit, and $n_{I,k}$ and $n_{Q,k}$ are samples of zero-mean Gaussian white noise sequences. The average phase over the kth interval, $\bar{\varphi}_k$, is related to the true and estimated phase sequences over the kth interval by

$$\bar{\varphi}_k = \frac{1}{N_k}\sum_{j=j_k}^{j_k+N_k-1}\theta(t_j) - \hat{\theta}(t_j) \quad (5)$$

Assuming $T_a >> 2\pi/\omega_{IF}$, the following statistics apply to $n_{I,k}$ and $n_{Q,k}$:

$$E[n_{I,k}n_{I,i}] = E[n_{Q,k}n_{Q,i}] = \left(\frac{N_k\sigma^2_{n_i}}{2}\right)\delta_{k,i} \equiv \sigma^2_{IQ}\delta_{k,i} \quad (6a)$$

$$E[n_{I,k}n_{Q,i}] = 0 \quad \text{for all} \quad k, i \quad (6b)$$

where $\delta_{k,i}$ is the Kronecker delta function.

In this study, four phase detector characteristics (discriminators) will be considered within the Costas-loop framework:
1. Arctangent (AT): $e_k = \arctan(Q_k/I_k)$
2. Conventional Costas (CC): $e_k = Q_k \cdot I_k$
3. Decision-Directed (DD): $e_k = \text{sign}(I_k) \cdot Q_k$
4. The KFPLL's implicit discriminator;

where e_k is the phase detector error signal.

In what follows, the CC discriminator is used to develop the baseband model of the Costas loop. A similar development involving decision error probability is possible for the DD discriminator (Ref. [12], ch. 2). Simulation will show that the behavior of the DD, AT, and KFPLL discriminators resembles that of the CC discriminator.

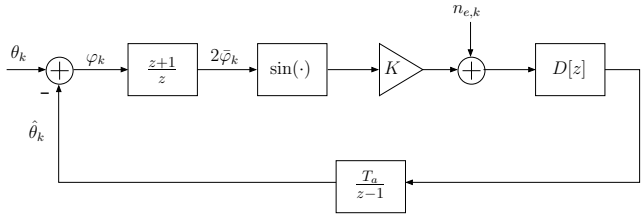

Fig. 2. Discrete-time baseband model of the Costas loop; $K = N_k^2\bar{A}_k^2/8$.

A.1 Baseband Model

The error signal for the CC discriminator is the product of I_k and Q_k:

$$e_k = I_kQ_k = \frac{N_k^2\bar{A}_k^2}{8}\sin(2\bar{\varphi}_k) + n_{e,k} \quad (7)$$

where use has been made of $m_l^2 = 1$ and where the signal×noise and noise×noise components of the error signal have been collected into the noise term $n_{e,k}$. The statistics of $n_{e,k}$ are found by applying Eqs. (6a) and (6b) to the noise terms of the $I_k \cdot Q_k$ product:

$$E[n_{e,k}] = 0 \quad (8a)$$

$$E[n_{e,k}n_{e,i}] = \left[\frac{N_k^2\bar{A}_k^2}{4}\sigma^2_{IQ} + \sigma^4_{IQ}\right]\delta_{k,i} \quad (8b)$$

The discrete-time transfer function $D[z]$ filters e_k to produce v_k, the control signal input to the numerically controlled oscillator (NCO). The NCO generates a sinusoid sampled every T_s seconds whose phase is related to v_k by

$$\hat{\theta}(t_j) = \hat{\theta}_k + (t_j - t_k)v_k, \quad t_k < t_j \leq t_{k+1} \quad (9a)$$

$$\hat{\theta}_{k+1} = \hat{\theta}_k + T_a v_k, \quad (9b)$$

Here, j denotes the index of samples taken at T_s whereas k denotes the index of samples taken at the accumulation interval, T_a. The average phase error over the accumulation interval from t_{k-1} to t_k is approximately related to the true and estimated phases by

$$\bar{\varphi}_k = \frac{\theta_{k-1} + \theta_k}{2} - \frac{\hat{\theta}_{k-1} + \hat{\theta}_k}{2} = \frac{\varphi_k + \varphi_{k-1}}{2} \quad (10)$$

where $\varphi_k = \theta_k - \hat{\theta}_k$.

Equations (7), (9b), and (10) suggest the baseband functional diagram presented in Fig. 2, with $K = N_k^2\bar{A}_k^2/8$. The baseband model retains the essential behavior of the

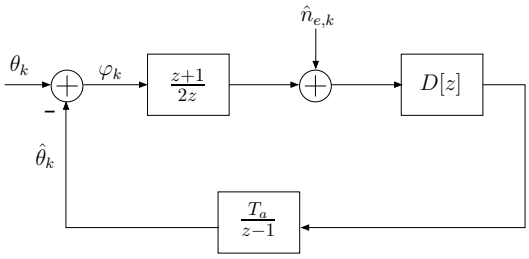

Fig. 3. Discrete-time constant-bandwidth linear model of the Costas loop.

Costas loop; namely, those effects associated with n_e, T_a, and $\sin(\cdot)$. Note that the baseband model presented here is different from those presented in Refs. [12, 14, 16–19] in that the present model explicitly accounts for the finite pre-detection bandwidth via the $[(z+1)/z]$ block. As will be shown subsequently, the effects of this block can be significant when the pre-detection bandwidth $1/T_a$ is near the loop bandwidth.

A.2 Linear Loop Operation

Consider two further simplifications of the baseband Costas loop model: (1) assume that the loop is tightly tracking so that $\sin(x) \simeq x$, and (2) assume that a gain factor of $4/N_k^2 A_k^2$ is added to the loop so that the gain parameter K is normalized to $K = 1/2$. For the CC and DD discriminators, the latter operation requires estimation of the average carrier amplitude $\bar{A}_k$; for the AT discriminator the normalization is automatic. The bandwidth of the resulting linearized loop (Fig. 3) is a constant that is set by the loop filter $D[z]$ and the accumulation interval T_a. The normalized noise $\hat{n}_{e,k} = 4n_{e,k}/N_k^2\bar{A}_k^2$ has mean 0 and variance

$$E[\hat{n}_{e,k}\hat{n}_{e,i}] = \left(\frac{4}{N_k^2\bar{A}_k^2}\right)^2 \left[\frac{N_k^2\bar{A}_k^2}{4}\sigma_{IQ}^2 + \sigma_{IQ}^4\right]\delta_{k,i} \equiv \sigma_{\hat{n}_e}^2\delta_{k,i} \tag{11}$$

The loop transfer function $H[z]$ and the loop noise transfer function $H_n[z]$ (from noise to phase estimate) can be written by inspection from Fig. 3 as

$$H[z] = \frac{\left(\frac{z+1}{2z}\right)\left(\frac{T_a}{z-1}\right)D[z]}{1 + \left(\frac{z+1}{2z}\right)\left(\frac{T_a}{z-1}\right)D[z]} \tag{12}$$

$$H_n[z] = \frac{\left(\frac{T_a}{z-1}\right)D[z]}{1 + \left(\frac{z+1}{2z}\right)\left(\frac{T_a}{z-1}\right)D[z]} \tag{13}$$

It is useful to calculate the phase error variance $\sigma_\varphi^2 = E[\varphi_k^2]$ as a function of input noise. (Here φ_k is assumed to be a stationary random sequence; hence σ_φ^2 does not depend on k.) Let $H(s)$ and $H_n(s)$ be the continuous-time equivalents of $H[z]$ and $H_n[z]$, and let $S_{\hat{n}_e} = T_a\sigma_{\hat{n}_e}^2$ be the power spectral density associated with the noise process $\hat{n}_{e,k}$. Equations (3), (6a), and (11) can be used to relate $S_{\hat{n}_e}$ to C/N_0:

$$S_{\hat{n}_e} = \frac{N_0}{2C}\underbrace{\left(1 + \frac{N_0}{2CT_a}\right)}_{\mathcal{S}_\mathcal{L}^{-1}} = \frac{N_0}{2C\mathcal{S}_\mathcal{L}} \tag{14}$$

The quantity $\mathcal{S}_\mathcal{L}$ in Eqs. (14) and (15) is termed the squaring loss and represents the penalty paid, relative to the standard PLL, for multiplying the I_k and Q_k accumulations together to remove the data bits. The variance in the output phase error is then given by

$$\sigma_\varphi^2 = \int_{-\infty}^{\infty} |H_n(f)|^2 S_{\hat{n}_e}(f)df = \frac{N_0 B_n}{C\mathcal{S}_\mathcal{L}} \tag{15}$$

where

$$B_n \equiv \int_0^\infty |H_n(f)|^2 df \tag{16}$$

is the one-sided bandwidth (in Hz) of $H_n(s)$. Note that the phase error variance is determined by B_n and not by the one-sided loop bandwidth B_L, which is defined as

$$B_L \equiv \int_0^\infty |H(f)|^2 df \tag{17}$$

The noise bandwidth B_n approaches B_L for small $B_L T_a$ (that is, when the pre-detection bandwidth $1/T_a$ is much larger than B_L), but this condition may not hold for receivers used in scintillation monitoring. This point is elaborated in the following section. Like B_n, $\mathcal{S}_\mathcal{L}$ is dependent on T_a. For 100-Hz accumulations ($T_a = 10$ ms), $\mathcal{S}_\mathcal{L}$ is near unity above $C/N_0 = 45$ dB-Hz, but at $C/N_0 = 20$ dB-Hz, $\mathcal{S}_\mathcal{L}$ increases σ_φ^2 by 50% relative to the standard PLL. Hence, at low C/N_0 the squaring loss severely degrades a receiver's phase accuracy, leading to loss of phase lock.

A.3 Remarks on Optimality

Considerable effort in prior research has focused on determining the Costas loop configuration that minimizes σ_φ^2. In Ref. [12], ch. 11 and Refs. [19, 20], it is shown that for $T_a = T_b$, the maximum *a posteriori* (MAP) phase estimator for bi-phase modulated signals with known symbol timing is a Costas-type loop with accumulate-and-dump arm filters and a discriminator given by $e_k = \tanh(\gamma I_k)\cdot Q_k$, where γ is a normalizing constant. Reference [19] shows that the MAP estimator also maximizes $\mathcal{S}_\mathcal{L}$, thereby minimizing σ_φ^2. The DD and CC discriminators considered in this paper are special cases of the tanh discriminator for high and low C/N_0. It can be shown that the approximation

$$\tanh(x) \simeq \begin{cases} x & \rho_a \le 0 \text{ dB (CC)} \\ \text{sign}(x) & \rho_a > 0 \text{ dB (DD)} \end{cases} \tag{18}$$

yields loop performance that is indistinguishable from that of the MAP loop.[19] The signal-to-noise ratio at the output of the accumulators, $\rho_a = 2CT_a/N_0$, determines the

choice between CC and DD. For practical GPS receiver operation, $\rho_a > 0$ dB (for example, for $C/N_0 \geq 15$ dB-Hz and $T_a = 0.02$ s, $\rho_a \geq 1.02$ dB). Hence, the DD discriminator is practically optimal. Although this result assumes $T_a = T_b$, simulation demonstrates that the DD discriminator outperforms the AT and CC discriminators for all T_a of interest.

Besides optimizing the loop structure and discriminator, one may further consider optimizing the loop filter $D[z]$. This has been done using Wiener Filtering Theory for the special case of small phase error and additive white noise with a time-invariant noise density.[11] In this case, the optimum zeroth-, first-, and second- order filters are those constant-coefficient filters presented in Refs. [17,18]. These are considered the standard PLL loop filters for GPS tracking loops. But a constant-coefficient loop filter may not be suitable for tracking carrier phase through the deep power fades associated with equatorial scintillations. Furthermore, the structure of the loop filters in Refs. [17,18] does not exploit what is known about the phase noise introduced by the receiver clock. In a later section, a Kalman-filter-based loop filter with a time-varying bandwidth and an explicit receiver clock error model is introduced.

Choice of PLL order may also be tailored to the problem of tracking scintillating signals. Many GPS receivers, including the ISM, employ a 3rd-order loop capable of tracking a ramping Doppler shift. This tracking ability could be traded for the added robustness of a lower-order loop. A study along these lines will be left for future work. In this paper, attention will be restricted to 3rd-order tracking loops.

A final consideration in the design of an accurate and robust carrier tracking loop is the accumulation interval, T_a. In loop design and analysis, it is commonly assumed that T_a is short enough that the pre-detection bandwidth $1/T_a$ is much wider than the loop bandwidth B_L.[17,18] Under this assumption, the accumulation interval has a negligible effect on the tracking loop's bandwidth and stability. In contrast, if $1/T_a$ is near B_L then a loop based on the standard continuous-time loop filters from Refs. [17,18] tends to destabilize, increasing the noise bandwidth B_n. The situation is illustrated in Fig. 4, which plots the loop noise transfer function of a standard 3rd-order loop with an equivalent continuous-time bandwidth of 15 Hz that is updated at three different accumulation intervals, $T_a = 1$, 10, and 20 ms, with corresponding pre-detection bandwidths of 1000, 100, and 50 Hz. As is evident, the longer accumulation intervals (10 and 20 ms) significantly increase the loop noise bandwidth B_n. Such an increase in the loop noise bandwidth can be mitigated by designing the loop filter directly in the digital domain instead of simply converting the standard continuous-time loop filters to their discrete-time approximations, but it must be recognized

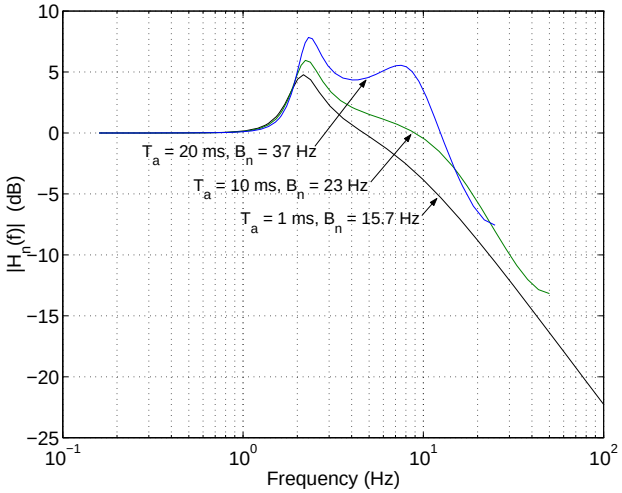

Fig. 4. Loop noise transfer function magnitude $|H_n(f)|$ for several values of T_a.

that, in general, B_n increases with increasing T_a. This is a standard result from discrete-time loop theory, but it bears repeating here because one might otherwise be tempted to conclude from Eq. (14) that T_a should be made as large as possible in order to reduce ${\mathcal{S}_{\mathcal{L}}}^{-1}$. One must bear in mind that the phase error variance $\sigma_\varphi^2 = N_0 B_n / C\mathcal{S}_{\mathcal{L}}$ [Eq. (15)] is dependent both on squaring loss and on loop noise bandwidth. Hence, T_a must be chosen to suitably trade off the noise contribution of each.

A.4 Nonlinear Effects and Threshold Behavior

When C/N_0 at the loop input drops below a certain level (as a result, for example, of a power fade caused by scintillation), there is a sudden deterioration in loop performance. In this threshold region, squaring loss and the nonlinear effects associated with $\sin(\cdot)$ begin to dominate loop behavior, eventually leading to a loss of phase lock.

Total loss of phase lock is preceded by cycle slipping. The cycle slip phenomenon can be understood by expressing the baseband model of Fig. 2 as a nonlinear stochastic difference equation. The baseband model's $\sin(2\bar{\varphi}_k)$ function is insensitive to phase error shifts of $n\pi$, where n is an integer. As a result, an infinite set of stable attractors exists for the nonlinear difference equation. The noise process $n_{e,k}$ can cause the phase error to slip from one attractor to another, leading to infinite σ_φ^2 in the steady-state. This is the familiar cycle slip phenomenon associated with PLLs. The effect is illustrated in Fig. 5. Note that for a constant waveform PLL (no data bit modulation on the incoming signal), a cycle slip is a phase error shift of $n \cdot 2\pi$; that is, an integer number of full carrier cycles. In contrast, the Costas-type PLL slips by half carrier cycles, making slippage more likely. In this paper, half cycle slips are referred to as cycle slips.

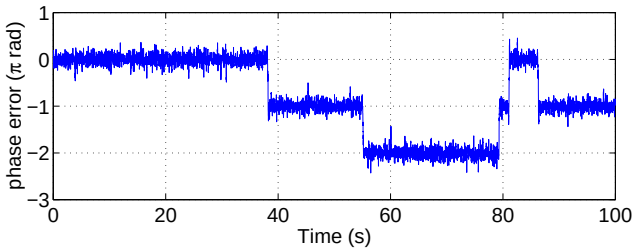

Fig. 5. Cycle slipping in a 2nd-order Costas loop with $B_L = 15$ Hz and $C/N_0 = 25$ dB-Hz.

Total loss of phase lock occurs when the tracking loop slips several cycles at once so that the difference between the true carrier frequency and the loop filter's internal estimate of carrier frequency falls outside the loop's frequency pull-in range (for 2nd- and 3rd order loops). A GPS receiver will declare loss of lock based on its code- and phase-lock detectors. A phase detector declares loss of lock when the phase error exceeds a predetermined threshold,[17] a condition that may preempt a total loss of lock within the tracking loop. Repeated data bit parity failure is the final indicator of loss of lock.

In order to characterize the complete statistics of φ_k, including cycle slips, one must calculate the pdf of φ_k directly from the nonlinear difference equation. A simpler strategy considers the pdf of ϕ_k, which is defined as φ_k reduced modulo 2π, and accounts for cycle slipping separately by a diffusion coefficient.[12] Analysis along these lines has been carried out for first- and second-order digital PLLs,[16,21] but becomes difficult at higher orders and in cases where $T_a B_L$ is not small. One may alternatively characterize the variance of ϕ_k and the mean cycle slip rate by simulation. This is the approach taken herein.

B. The Kalman Filter-based PLL

The possibility of using a variable-bandwidth loop filter to track scintillating GPS signals was mentioned in the discussion on loop optimization. In this section, a Kalman filter-based phase-locked loop (KFPLL) is proposed as one such variable-bandwidth strategy. This approach is attractive because the bandwidth chosen by the Kalman filter represents the optimal bandwidth in the sense that σ_φ^2 is minimized under the assumption of additive white Gaussian noise. Earlier applications of the Kalman filter to PLLs are reported in Refs. [11, 23] and references therein. These estimators have a time-varying Kalman gain, and consequently a time-varying bandwidth, but they are suboptimal in the sense that they solve only the steady-state Ricatti equation. Moreover, they are not designed to track a carrier signal that is fully modulated by data bits (suppressed carrier). In contrast, the Kalman filter developed in Ref. [24] and summarized here is a full implementation of the extended Kalman filter that is specially designed for tracking weak suppressed-carrier GPS signals.

Proper choice of loop bandwidth requires the KFPLL to continuously estimate C/N_0. Accordingly, the KFPLL's state vector includes an estimate of carrier amplitude along with estimates of carrier phase, Doppler shift, and Doppler rate. The KFPLL's state $\boldsymbol{x}_k$ at time t_k is related to its state at time t_{k+1} by the dynamics model

$$\boldsymbol{x}_{k+1} = \Phi_k \boldsymbol{x}_k + \boldsymbol{u}_k + \boldsymbol{w}_k \tag{19}$$

where $\boldsymbol{u}_k$ is a control input from the receiver's NCO and $\boldsymbol{w}_k$ is the process noise made up of contributions from the receiver clock errors, line of sight acceleration changes (jerk), and varying signal amplitude. Equation (19) includes a discrete-time triple integrator driven by white noise for the update of the phase elements and a random walk model for the carrier amplitude update. Both the noise models and the state transition matrix Φ_k depend on T_a. However, simulation demonstrates that, in contrast to the CBPLLs, the phase error variance of the KFPLL is relatively insensitive to changes in T_a.

Equations (4a) and (4b), with $\bar{\varphi}_k = \bar{\varphi}_k(\boldsymbol{x}_k, \boldsymbol{u}_k, \boldsymbol{w}_k)$, constitute the KFPLL's nonlinear measurement model. The KFPLL deals with the unknown data bits in the measurement equation by running two separate estimators in parallel. One estimator propagates the state and performs a measurement update under the assumption that $m_l = 1$; the other estimator does the same under the assumption that $m_l = -1$. A Bayesian analysis based on carrier phase and amplitude innovations is used to estimate the relative probabilities of the $+1$ and -1 data bit signs. These relative probabilities, in turn, are used to synthesize an overall state estimate whose elements drive the PLL feedback loop.

The KFPLL may be thought of as a Costas-type tracking loop with a variable bandwidth and a soft-decision discriminator. It adjusts its bandwidth based on its models for process noise $\boldsymbol{w}_k$ and measurement noise $n_{I,k}$ and $n_{Q,k}$. Because the measurement noise depends on C/N_0, the KFPLL bandwidth varies as a function of C/N_0.

One can determine the KFPLL's effective noise bandwidth B_n by Monte-Carlo simulation. Low-intensity noise ($C/N_0 > 45$ dB-Hz) is fed to the KFPLL while its internal estimate of C/N_0 is artificially varied. The variance of the resulting phase error is then estimated and related to B_n by Eq. (15). Use of low-intensity noise ensures that the linearity assumptions underlying Eq. (15) are valid. Figure 6 shows an example B_n vs. C/N_0 curve for mild line-of-sight dynamics and receiver clock errors typical of a temperature-compensated crystal oscillator (TCXO).

Characterization of the KFPLL's phase detector characteristic as a "soft-decision" discriminator is based on a comparison with the DD discriminator. Whereas the DD

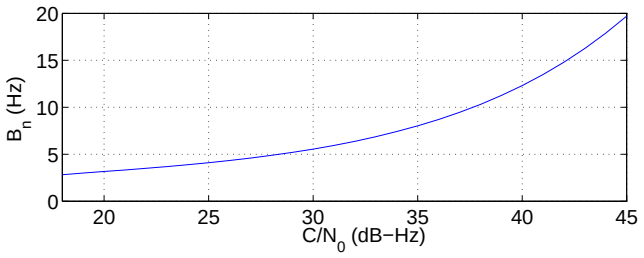

Fig. 6. KFPLL effective noise bandwidth as a function of C/N_0.

discriminator measures carrier phase by making a hard decision about the sign of the current data bit, the KFPLL weights two alternative phase estimates, one for each bit sign, by the *a posteriori* probabilities for each bit sign, thereby reflecting uncertainty about the current data bit in the phase estimate update.

Note that the KFPLL is a causal estimator; that is, it operates only on past measurements. Hence, given sufficient processing capability, the KFPLL can be used for real-time ionospheric monitoring applications.

II. SIMULATION

A. Simulation Setup

A Matlab equivalent of the baseband Costas loop model of Fig. 2 was created for each of the AT-, CC-, and DD-based CBPLLs. The KFPLL was likewise implemented in Matlab. The loop filter $D[z]$ for the CBPLLs is the discrete-time equivalent of the 2nd-order loop filter presented in Refs. [11] and [18]. This is considered the standard 2nd-order PLL loop filter. The resulting feedback loop is 3rd-order. The CC and DD loops have been normalized as discussed in Section I-A.2 so that their loop gains are equivalent to that of the AT loop.

Independent Gaussian noise samples are added to the I_k and Q_k accumulations to simulate loop noise. For comparative tests, each PLL is fed with the same noise sequence. The noise variance is related to C/N_0 by Eqs. (3) and (6a), but can be expressed more conveniently for baseband simulation as

$$\sigma_{IQ}^2 = \frac{[I^2+Q^2]_{nom}}{2T_a C/N_0} \tag{20}$$

where $[I^2+Q^2]_{nom}$ is the squared magnitude of the nominal (noise-free) (I,Q) vector. To simulate the loss of power that results from a change in phase error over the accumulation interval, the nominal (I,Q) vector magnitude is scaled by the factor $2\sin(\bar{\varphi}_k/2)/\bar{\varphi}_k$ before noise is added to the accumulations.

The tracking loop implementations have been configured so that T_a can be chosen from the set $\{1,2,4,5,10,20\}$ ms. Because the KFPLL makes use of all the accumulations within a bit interval to arrive at its bit sign probabilities, the DD-discriminator loop has been likewise configured so that the sign$(\cdot)$ function operates on the sum of the in-phase accumulations within each bit interval.

Three cases of true phase dynamics are considered. Case 0 assumes no phase dynamics ($\theta_k = 0$ for all k), which implies a constant line of sight separation and a perfect receiver clock. Case I assumes phase dynamics consistent with a 7×10^{-4}-g change in line of sight acceleration in 10 seconds (roughly 30 times the maximum jerk experienced by a stationary receiver on the Earth's surface) and a receiver clock with a TCXO frequency reference. Case II is like Case I except that the frequency reference is assumed to be an ovenized crystal oscillator (OXO) instead of a TCXO.

B. Simulation Results

B.1 The AT, CC, and DD CBPLLs

Parameter values for the CBPLLs were chosen to match those of the ISM: continuous-time $B_L = 15$ Hz; $T_a = 10$ ms.[9] For Case 0 true phase dynamics, a log-scale comparison of the phase error standard deviation over a range of C/N_0 is presented in Fig. 7. Five Monte-Carlo simulations were used to generate σ_φ estimates over the range $29 \le C/N_0 \le 45$ dB-Hz. No cycle slips occurred in this region. Within the threshold region (25 to 28 dB-Hz), 50 Monte-Carlo trials were required because cases with cycle slips or loss of lock were not included in the σ_φ estimate. Figure 7 includes results from the AT-, CC-, and DD- discriminator loops as well as the phase deviation predicted by linear theory for the CC-discriminator [Eq. (15)]. The coincidence of the plots above $C/N_0 = 30$ dB-Hz reflects the accuracy of the linear approximation for moderate to high C/N_0.

A linear-scale view of the threshold region is shown in Fig. 8. As anticipated, the loops' phase deviations diverge from the linear theory prediction in the threshold region. Note that below 29 dB-Hz the DD deviation is lower than that predicted by linear theory. By estimating the data bit sign, the DD discriminator avoids part of the noise×noise term that causes squaring loss.

Cycle slip statistics at several values of C/N_0 in the threshold region are presented in Fig. 9. The plot shows the probability of either a cycle slip or a total loss of lock during a 20-second interval at each C/N_0. Probabilities were calculated using data from 300 Monte-Carlo runs at each value of C/N_0. The DD discriminator has a decided advantage at each particular C/N_0, but in practical terms its lock threshold is only about 1.5 dB lower than that of the AT discriminator. Comparison of Figs. 8 and 9 confirms the rule of thumb that a cycle slip is imminent when σ_ϕ exceeds 15 deg.[18]

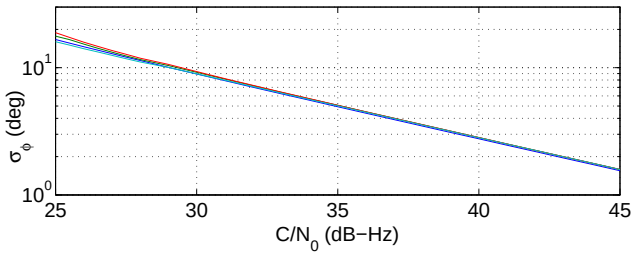

Fig. 7. Phase error vs. C/N_0 for target $B_L = 15$ Hz and $T_a = 10$ ms.

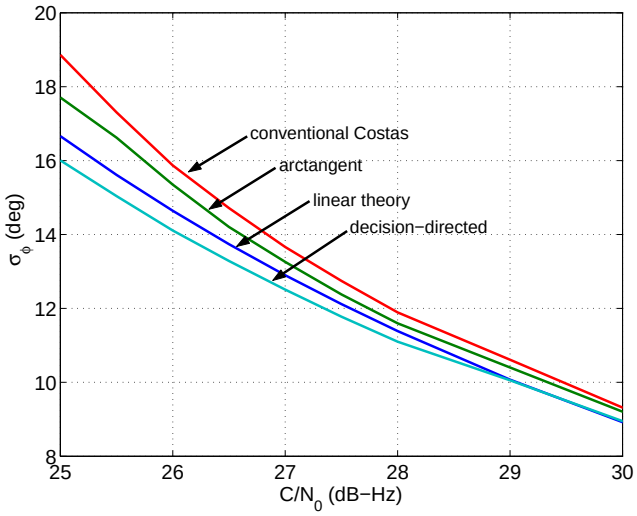

Fig. 8. Threshold-region phase error standard deviation vs. C/N_0 for target $B_L = 15$ Hz and $T_a = 10$ ms.

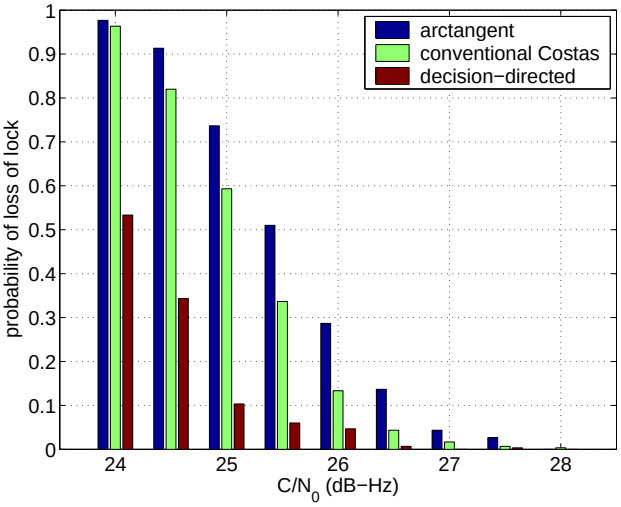

Fig. 9. Probability of loss of lock over a 20-second interval at several values of C/N_0 in the threshold region. Target $B_L = 15$ Hz and $T_a = 10$ ms.

A hybrid decision-directed arctangent discriminator modeled after the one employed by the ISM[4,9] was also tested in comparison to the DD, CC, and AT discriminators. This discriminator makes use of the four-quadrant arctangent function atan2$(\cdot,\cdot)$ that is usually reserved for the continuous-wave PLL (no modulating data bits).[18] As with the DD discriminator, the 180-deg phase shifts caused by data bit transitions are eliminated by estimating the current data bit as the sign of $I_{l,k}$, the sum of the in-phase accumulations in the current data bit interval. Hence, for the hybrid decision-directed arctangent discriminator

$$e_k = \text{atan2}\left[\text{sign}(I_{l,k}) \cdot Q_k, \text{sign}(I_{l,k}) \cdot I_k\right] \qquad (21)$$

The hybrid discriminator is equivalent to the AT discriminator when $T_a = 20$ ms; that is, when only one accumulation occurs per data bit. Simulation shows that for $T_a = 10$ ms the phase error performance of the hybrid discriminator is slightly better than the AT and CC discriminators, but worse than the DD discriminator. Because these simpler discriminators provide bounds on the hybrid discriminator's performance, the latter will not be treated further in this section.

Figure 9 has bearing on the problem of tracking scintillating GPS signals. During strong equatorial scintillations, C/N_0 can plummet by more that 20 dB and remain low for seconds. For a typical quiescent C/N_0 of 45 dB-Hz, such a signal fade would force a 15-Hz tracking loop to operate near 25 dB-Hz—at the lower boundary of its threshold region. The low squaring loss of the DD discriminator offers some relief, but a more dramatic reduction in lock threshold requires a reduction in loop bandwidth. For example, the lower boundary of a 3-Hz loop's threshold region is around 20 dB-Hz. A 15-Hz loop cannot be expected to operate reliably during strong equatorial scintillations. This proposition is corroborated subsequently using actual scintillating GPS signals.

Lowering the loop bandwidth enables a PLL to maintain lock on weak signals, but there is a penalty to be paid: the loop is no longer able to respond to vigorous phase scintillations. When phase scintillations are not accompanied by amplitude fades (as is typically the case for auroral scintillations[5,6]), the PLL bandwidth should be made wide enough to accurately track the phase scintillations. Ideally, a phase-tracking loop should be agile when tracking auroral scintillations and sluggish when tracking equatorial scintillations. This is the motivation behind the variable-bandwidth KFPLL.

B.2 Comparison of the CBPLLs and the KFPLL

To evaluate the performance of the KFPLL in comparison to the CBPLLs over the range of C/N_0 shown in Fig. 7, the noise bandwidth of the CBPLLs was matched at each C/N_0 to that of the KFPLL. Neither the CBPLLs nor the KFPLL experienced cycle slips for $25 \leq C/N_0 \leq 45$

dB-Hz under these conditions. By this procedure it was found that the KFPLL's phase error variance is approximately equal to that of the DD CBPLL and slightly better than that of the AT and CC CBPLLs. This implies that the squaring loss associated with the KFPLL's implicit soft-decision discriminator is effectively equivalent to the squaring loss of the DD discriminator.

The advantage of the KFPLL over the CBPLLs becomes more apparent near the KFPLL's lock threshold and when the true phase dynamics are non-zero. Consider a KFPLL whose internal process noise model assumes phase dynamics like those of Case I and also assumes vigorous amplitude dynamics that allow a 100% change in signal amplitude in 1/7th of a second. Such a KFPLL is tuned to operate in the presence of ionospheric scintillations with a low-cost frequency reference.

The KFPLL's lock threshold for Case I true phase dynamics is near $C/N_0 = 19$ dB-Hz. At this value of C/N_0 the KFPLL's effective noise bandwidth is 3 Hz. For Case II true phase dynamics, the lock threshold is near $C/N_0 = 21$ dB-Hz and the effective noise bandwidth is 3.5 Hz. For a comparative evaluation, the noise bandwidths of the AT, CC, and DD CBPLLs were tuned to match the noise bandwidth of the KFPLL at $C/N_0 = 19$ and at 21 dB-Hz, and T_a for all PLLs was set to 0.02 seconds. Statistics from 3000 20-second intervals were used to calculate mean time to loss of lock, where loss of lock is defined as either a cycle slip or a total loss of lock. Results are given in Table I, with error bounds indicating 1σ confidence intervals.

TABLE I
MEAN TIME TO LOSS OF LOCK (SECONDS)

PLL	True phase: Case 0 $C/N_0 = 19$ dB-Hz	True phase: Case I $C/N_0 = 21$ dB-Hz
AT	86 ± 2	18.7 ± 0.3
CC	686 ± 45	10.4 ± 0.2
DD	700 ± 36	28.7 ± 0.8
KF	1207 ± 105	433 ± 33

The test results indicate that the KFPLL's mean time to loss of lock for Case 0 true phase dynamics at $C/N_0 = 19$ dB-Hz is roughly twice that of the best CBPLL with an equivalent noise bandwidth. For Case I true phase dynamics at $C/N_0 = 21$ dB-Hz, the KFPLL's advantage is much more pronounced: it's mean time to loss of lock is more than ten times that of the best bandwidth-equivalent CBPLL. The KFPLL appears to deal more effectively than the CBPLLs with the $\sin(\cdot)$ nonlinearity, whose effects become dominant in the threshold region. Similar matched-bandwidth tests with C/N_0 ranging from 19 to 24 showed that the KFPLL's practical advantage for Case 0 is slight—it's lock threshold is less than 1 dB below that of the best bandwidth-equivalent CBPLL. On the other hand, for the more realistic Case I dynamics the KFPLL's lock threshold is a substantial 3 dB below that of the best bandwidth-equivalent CBPLL.

Of course, the primary advantage of the KFPLL is not that it outperforms a matched-bandwidth CBPLL, but that it optimally adapts its bandwidth to C/N_0. To see this, one can convert the probabilities in Fig. 9 to mean time to loss of lock to show that the KFPLL's lock threshold is more than 7 dB below the 15-Hz CBPLL's lock threshold for Case 0 phase dynamics.

B.3 KFPLL enhancement and further applications

It is possible to extend the KFPLL's Bayesian treatment of the current data bit to include the past N_b data bits. This requires a bank of 2^{N_b} parallel Kalman filters, one for each of the different possible combinations of recent data bits, which entails a 2^{N_b-1}-fold increase in computation.

In addition, one might consider operation of the KFPLL under more favorable circumstances than using a low-cost TCXO frequency reference in the presence of strong ionospheric scintillations. For example, suppose that line of sight jerk remains the same as in Case I but that an OXO frequency reference is used instead of a TCXO. This situation corresponds to Case II true phase dynamics. Further assume that signal amplitude changes are benign: a 100% amplitude change now requiring 1000 seconds. Table II compares the KFPLL's mean time to cycle slip for this case at several different values of N_b, where means and 1σ error bounds were computed as for Table I. A matched-bandwidth DD CBPLL, chosen to represent the best of the CBPLLs, is included for reference. The effective noise bandwidth is 0.65 Hz.

TABLE II
MEAN TIME TO LOSS OF LOCK (SECONDS)

PLL	N_b	True phase: Case II $C/N_0 = 15$ dB-Hz
DD	N/A	157 ± 5
KF	1	3546 ± 222
KF	2	4435 ± 556
KF	3	3768 ± 222
KF	4	4435 ± 556
KF	5	4991 ± 962

It is apparent from Table II that the KFPLL convincingly outperforms the matched-bandwidth DD CBPLL at $C/N_0 = 15$ dB-Hz . The worst KFPLL mean time to loss of lock is more than 20 times longer than that of the DD PLL. It is also apparent that an increase in N_b leads to a slight but noticeable improvement in mean time to loss of lock. The KFPLL's ability to maintain lock with Case

II true phase dynamics at $C/N_0 = 15$ dB-Hz represents a significant performance improvement over the roughly 25-dB-Hz threshold of the 15-Hz CBPLLs (cf. Fig. 9) with Case 0 true phase dynamics (which assume a perfect receiver clock and no line of sight dynamics).

III. TRACKING LOOP EVALUATION USING ACTUAL GPS DATA

The performance of the AT CBPLL and the KFPLL was also evaluated using real GPS signals. The AT discriminator was chosen because it does not require loop gain normalization, making it a common choice for many tracking loop implementations. The ISM's hybrid decision-directed arctangent discriminator was also tested.

The input data are wideband GPS L1 C/A code digital data sampled at 5.7 MHz that were recorded in Cachoeira Paulista, Brazil from December 4 to 6, 2003.[7] Cauchoeira Paulista lies along the southern boundary of the Appleton equatorial anomaly. This region is notorious for strong ionospheric scintillations.[25,26] The recorded data set spans several hours and includes scintillations with S_4 index values greater than 0.9 that are associated with power fades of more than 30 dB. The digital storage device used to record the GPS data is equipped with a TCXO. Consequently, the sampling rate of the recorded wideband data is affected by the TCXO's frequency instability. This is discussed further in the next section.

An FLL-based real-time Cornell scintillation monitor was co-located with the digital storage device during the campaign in Brazil. The FLL-based monitor lost lock many times during strong scintillations. These loss of lock times were used to guide a selection of data intervals over which the KFPLL and AT CBPLL were evaluated. Figures 10 and 11 present one such interval over which the S_4 index exceeds 0.9.

The C/N_0 estimate shown in Fig. 10 is based on the KFPLL's signal amplitude estimate over the interval and on a noise floor estimate taken from a simulaneously available non-scintillating GPS signal. The KFPLL maintains lock throughout the interval. In contrast, the AT CBPLL, with continuous-time $B_L = 15$ Hz and $T_a = 10$ ms, experiences a total loss of lock at the point indicated on the C/N_0 estimate in Fig. 10. The deep C/N_0 fade that occurs at this point causes the loss. A CBPLL based on the hybrid decision-directed arctangent discriminator also experiences a loss of lock, but re-acquires after a lapse of approximately 7 seconds. A 10-Hz version of the AT CBPLL does not experience a total loss of lock over the interval, but it does suffer cycle slips, as illustrated in Fig. 11. The cycle slips shown in the lower panel are relative to the KFPLL's phase estimate; nonetheless, an inspection of the top panel suggests that these slips also occur relative to the true carrier phase since the AT CBPLL's detrended

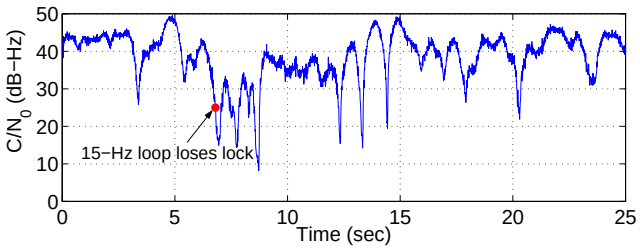

Fig. 10. KFPLL estimate of C/N_0 over an interval with $S_4 > 0.9$

.

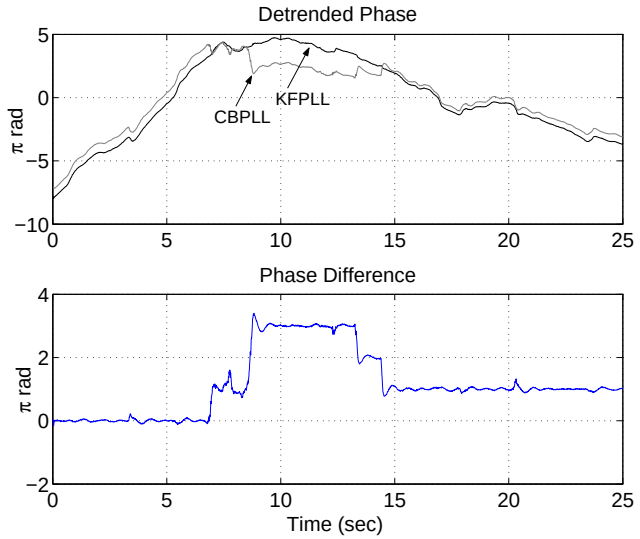

Fig. 11. Detrended phase and phase difference for the KFPLL and a 10-Hz AT CBPLL.

phase changes at the slippage points appear unphysical. A 5-Hz version of the AT CBPLL tracks the KFPLL's phase estimate closely, experiencing no relative cycle slips. Close inspection of the KFPLL phase estimate in the top panel of Fig. 11 reveals that even the KFPLL (and the 5-Hz AT CBPLL) may also experience one 1-π cycle slip over the interval. In no cases studied did the KFPLL or a $\leq$ 10-Hz AT CBPLL experience total loss of lock.

IV. REMARKS

The behavior of the KFPLL and the AT CBPLL when tracking the recorded scintillation data suggests that, for equatorial scintillations, loss of lock is caused by the low signal-to-noise ratios brought on by deep power fades. This is in contradistinction to the notion that loss of lock occurs because the limited PLL bandwidth does not permit tracking of high-frequency phase variations. Although one can construct a model of destructive phase interference that predicts rapid phase fluctuations during power fades, the low C/N_0 in these power fades makes the phase changes exceedingly difficult to track, regardless of the PLL bandwidth. The winning strategy for equatorial scintillations is to slog through the power fades using a low loop bandwidth

($\leq$ 5 Hz), ignoring the spurious phase changes brought on by destructive interference. This strategy is consistent with the findings of Ref. [10] and explains the good performance of the KFPLL's adaptive-bandwidth scheme and of the low-bandwidth AT CBPLL.

For auroral scintillations, phase variations—not power fades—are the dominant phenomenon.[5,6] Under such conditions, a high-bandwidth ($>$ 5 Hz) tracking loop is favored. No wideband data for auroral scintillations were available to the authors; however, one notes from Fig. 6 that the bandwidth of the KFPLL for $C/N_0 > 42$ dB-Hz is greater than 10 Hz and would be adequate for tracking auroral phase scintillations. This highlights the general applicability of the KFPLL.

Some cycle slipping during strong equatorial scintillations is perhaps unavoidable, even for low-bandwidth tracking loops. This suggests caution when interpreting phase sigmas, the common measure of phase scintillation.[3–5] Instead of measuring phase scintillation, one might be measuring cycle slips. A recorded phase history is required to distinguish the two effects.

As was mentioned in the foregoing section, the digital storage device used to record the GPS data employs a TCXO frequency reference. It has been shown that a TXCO's frequency instability is on the order of scintillation-induced carrier phase variations.[3,17] Hence, a TCXO introduces significant errors into a PLL's phase estimate. This is true for the CBPLLs and the KFPLL alike. (Even though the KFPLL's internal model of TCXO-induced phase errors enables it to more reliably maintain carrier lock, the KFPLL cannot distinguish between actual phase variations and TCXO-induced phase variations. Hence, its phase estimate is also corrupted by TCXO noise.) Despite the TCXO's poor frequency stability, its low cost makes it practical for use in large arrays of scintillation monitors. If a short latency in the provision of phase estimates is allowed, then the problem of TCXO-corrupted phase estimates can be overcome by estimating the TCXO-induced phase errors on a non-scintillating signal and subtracting this estimate from a scintillating signal's phase estimate.[3] This technique will be further developed in future work.

V. CONCLUSIONS

Costas-type phase-locked loops (PLLs) for use in GPS receivers have been analyzed and tested to evaluate their performance during ionospheric scintillations. Constant-bandwidth 15-Hz loops show adequate performance at moderate to high carrier-to-noise ratios, but experience cycle slips and total loss of phase lock at ratios below $\sim$26 dB-Hz. Use of the decision-directed phase discriminator improves phase accuracy and reduces the lock threshold by $\sim$ 1 dB relative to the conventional Costas and arctangent discriminators. A variable-bandwidth PLL based on a Kalman filter has also been tested. The Kalman filter-based PLL explicitly models the effects of receiver clock errors, optimally adapts its bandwidth to the carrier-to-noise ratio, and deals with data bit uncertainty by a Bayesian analysis of past data bits. In extensive simulation and in tests using actual scintillating GPS signals recorded in Brazil, the Kalman filter PLL demonstrated improved cycle-slip immunity relative to the constant-bandwidth PLLs. Because of its optimally-adapted bandwidth, the Kalman filter PLL offers accurate and robust phase and amplitude tracking for equatorial scintillations and is also expected to perform well in the presence of auroral scintillations.

ACKNOWLEDGMENTS

This work is supported by ONR grant number N00014-04-1-0105 and by the NASA Office of Space Science through grants No. NAG5-12211 and NAG5-12089. David Sibeck is the grant monitor for the latter grant. The authors would like to thank Dr. Eurico R. de Paula of INPE for his collaboration during the data-gathering campaign in Brazil.

References

[1] Beach, T. L. and Kintner, P. M., "Simultaneous Global Positioning System observations of equatorial scintillations and total electron content fluctuations," *Journal of Geophysical Research*, Vol. 104, 1999, pp. 22,553–22,565.

[2] Beach, T. L., *Global Positioning System Studies of Equatorial Scintillations*, Ph.D. thesis, Cornell University, Ithaca, N.Y., 1998.

[3] Van Dierendonck, A. J., Klobuchar, J., and Hua, Q., "Ionospheric Scintillation Monitoring Using Commercial Single Frequency C/A Code Receivers," *Proceedings of the 1993 ION GPS Conf.*, Portland, Oregon, 1993, pp. 1333–1342.

[4] Van Dierendonck, A. J. and Hua, Q., "Measuring Ionospheric Scintillation Effects from GPS Signals," *Proceedings of the 2001 ION Annual Meeting*, Albuquerque, New Mexico, 2001, pp. 391–396.

[5] Doherty, P. H., Delay, S. H., Vallardes, C. E., and Klobuchar, J. A., "Ionospheric Scintillation Effects in the Equatorial and Auroral Regions," *Proceedings of the 2000 ION GNSS Conf.*, Salt Lake City, Utah, 2000, pp. 662–671.

[6] Aarons, J., "Global positioning system phase fluctuations at auroral latitudes," *Journal of Geophysical Research*, 1997.

[7] Humphreys, T. E., Ledvina, B. M., Psiaki, M. L., and Kintner, P. M., "Analysis of Ionospheric Scintillations using Wideband GPS L1 C/A Signal Data," *Proc. 2004 ION GNSS Conf.*, Institute of Navigation, Long Beach, California, 2004, pp. 399–407.

[8] Van Dierendonck, A. J., "How GPS receivers measure (or should measure) ionospheric scintillation and TEC and how GPS receivers are affected by the ionosphere," *Proc. 11th International Ionospheric Effects Symposium*, Alexandria, VA, 2005.

[9] Van Dierendonck, A. J., private communication, November 2004.

[10] Morrissey, T. N., Shallberg, K. W., Van Dierendonck, A. J., Kim, T., and Nicholson, M. J., "GPS Receiver Performance Characterization Under Simulated Ionospheric Scintillation Environments," *Proceedings of the IAIN World Conference in association with the 56th ION Annual Meeting*, Institute of Navigation, Fairfax, VA, 2002, pp. 682–693.

[11] Gupta, S., "Phase-Locked Loops," *Proc. IEEE*, Vol. 63, No. 2, 1975, pp. 291–306.

[12] Lindsey, W. C. and Simon, M. K., *Telecommunication Systems Engineering*, Prentice-Hall, New Jersey, 1973.

[13] Lindsey, W. C., *Synchronization Systems in Communication and Control*, Prentice-Hall, New Jersey, 1972.

[14] Viterbi, A. J., *Principles of Coherent Communication*, McGraw-Hill, New York, 1966.
[15] Gardner, F. M., *Phase Lock Techniques*, Wiley, New York, 2nd ed., 1979.
[16] Lindsey, W. C. and Chie, C. M., "A Survey of Digital Phase-Locked Loops," *Proc. IEEE*, Vol. 69, No. 4, 1981, pp. 410–431.
[17] Van Dierendonck, A. J., *Global Positioning System: Theory and Applications*, chap. 8: GPS Receivers, American Institute of Aeronautics and Astronautics, Washington, D.C., 1996, pp. 329–407.
[18] Ward, P., *Understanding GPS: Principles and Applications*, chap. 5: Satellite Signal Acquisition and Tracking, Artech House, Boston, 1996, pp. 119–208.
[19] Simon, M. K., "On the optimality of the MAP estimation loop for carrier phase tracking BPSK and QPSK signals." *IEEE Transactions on Communications*, Vol. COM-27, No. 1, 1979, pp. 158–165.
[20] Simon, M. K. and Chie, C. M., "Optimum Performance of Suppressed Carrier Receivers with Costas Loop Tracking," *IEEE Transactions on Communications*, Vol. COM-25, No. 2, 1977, pp. 215–227.
[21] Fitz, M. P. and Cramer, R. J.-M., "A performance analysis of a digital PLL based MPSK demodulator," *IEEE Transactions on Communications*, Vol. 43, No. 2/3/4, 1995, pp. 1192–1201.
[22] Morrissey, T. N., Shallberg, K. W., Van Dierendonck, A. J., and Nicholson, M. J., "GPS receiver performance characterization under realistic ionospheric phase scintillation environments," *Radio Sci.*, Vol. 39, 2004, pp. 1–18.
[23] Statman, J. I. and Hurd, W. J., "An Estimator-Predictor Approach to PLL Loop Filter Design," *IEEE Transactions on Communications*, Vol. 38, No. 10, 1990, pp. 1667–1669.
[24] Psiaki, M. L. and Jung, H., "Extended Kalman Filter Methods for Tracking Weak GPS Signals," *Proceedings of the 2002 ION GPS Conf.*, Portland, Oregon, 2002, pp. 2539–2553.
[25] Aarons, J., "Global Morphology of Ionospheric Scintillations," *Proceedings of the IEEE*, Vol. 70, No. 4, 1982, pp. 360–378.
[26] Klobuchar, J. A., *Global Positioning System: Theory and Applications*, chap. 12: Ionospheric Effects on GPS, American Institute of Aeronautics and Astronautics, Washington, DC, 1996, pp. 485–515.